Optical properties of the Dead Sea

Emmanuel Boss,[1] Hezi Gildor,[2] Wayne Slade,[3] Leonid Sokoletsky,[4] Aharon Oren,[5] and James Loftin[1]

Received 1 November 2012; revised 28 December 2012; accepted 3 February 2013.

[1] The Dead Sea, located in the rift valley between Jordan and Israel, is a hypersaline lake, resulting in unique biogeochemistry and optical properties. In the spring of 2004 we conducted two days of physical and optical measurements in the lake. Because of the significant effect of dissolved salts on the optical properties of water, our analysis required a novel processing approach to obtain dissolved and total inherent optical properties from the measurements. In addition, we show that the lake's salinity can be estimated from measurements of hyper-spectral absorption or attenuation spectra in the red and infrared parts of the spectrum, using published values of specific absorption of dissolved NaCl, despite the fact that the lake's salt chemistry is complex. In situ observations demonstrated that the lake has a two-layer structure with a warm and more turbid layer at the top 20–30 m and a clearer colder layer below. Both the particulate and dissolved absorption are well approximated by exponentially decreasing functions with the spectral slope of the particulate absorption about half that of the dissolved fraction and consistent with other aquatic environments. Both have relatively low and similar magnitudes in the blue (O(0.15 m^{-1})). Mean particle size was observed to increase with depth, consistent with precipitating salt crystals (observed in past campaigns) shown here to play a major role in the lake's optical properties.

Citation: Boss, E., H. Gildor, W. Slade, L., Sokoletsky, A. Oren, and J. Loftin (2013), Optical properties of the Dead Sea, *J. Geophys. Res. Oceans*, *118*, doi:10.1002/jgrc.20109.

1. Introduction

[2] The Dead Sea, the lowest water body on Earth, is a hypersaline terminal lake located in the Jordan Rift Valley (Figure 1). The lake is 67 km long, up to 18 km wide, and 300 m in depth at its deepest point [*Gertman and Hecht*, 2002]. Diversion of fresh-water upstream the Jordan River since the 1960s and pumping of water into the ponds of Dead Sea Works and of the Arab Potash Company result in a negative water balance, and the lake surface level is dropping at an approximated rate of 1 m/yr (in 2005 the lake level was 418 meters beneath mean sea level, [*Gavrieli et al*., 2006]). As a consequence of evaporation, the salinity of the lake has been increasing [*Anati*, 1999; *Gertman and Hecht*, 2002]. The lake is extreme in its salinity (approximately 280 g kg^{-1}), and density (1236 kg m^{-3}; [*Gertman and Hecht*, 2002]) and, as a consequence of high salinity, almost completely lacks living organisms, except for infrequent and short periods of dense microbial blooms at time of fresh water input [*Oren*, 1999]. Indeed, since they were last detected in 1996, no algae were observed in the Dead Sea. Also, associated with the increase in salinity, since 1983 the lake has been precipitating salts, in particular NaCl [*Anati*, 1993; *Stiller et al*., 1997]. Due to selective input and removal of ions from the Dead Sea, its dissolved salts composition is different from that typical to oceans [*Gavrieli et al*., 1989; *Anati*, 1993].

[3] Suspended matter in the lake consists mainly of crystals of sodium chloride (halite) that spontaneously precipitate out of the water column [*Steinhorn*, 1983; *Anati*, 1993; *Gavrieli*, 1997; *Stiller et al*., 1997]. In addition, *Gavrieli* [1997] (and references therein) and *Stiller et al*. [1997] reported observations of suspended crystals of gypsum and aragonite, and a small component of detrital sediments (calcite, dolostone, limestone, quartz, feldspars, and clay minerals), which are input from dust deposition and rivers.

[4] The only optical data regarding the Dead Sea that has been published to date are three photosynthetically available radiation (PAR) irradiance depth profiles [*Oren and Shilo*, 1982]. Given this lack of optical characterization, a short field campaign was organized on 13–14 April 2004. The measurements presented special challenges, particularly with respect to the use of deionized water (DIW) as calibration fluid for the optical instruments used in the lake (dissolved salts affect water light attenuation as well as light transmission across the interface between water and instrument). Additional laboratory measurements of optical properties of a sample of Dead Sea waters collected in May 2012 allowed us to better understand the effects of salts on the field measurements and on the optical properties of the lake. Using the insight from

[1]School of Marine Science, University of Maine, Orono, Maine, USA.
[2]Institute of Earth Sciences, The Hebrew University of Jerusalem, Jerusalem, Israel.
[3]Sequoia Scientific, Bellevue, Washington, USA.
[4]State Key Laboratory of Estuary and Coastal Research, East China Normal University, Shanghai, China.
[5]Department of Plant and Environmental Sciences, The Hebrew University of Jerusalem, Jerusalem, Israel.

Corresponding author: E. Boss, School of Marine Science, University of Maine, Orono, ME 04473, USA. (emmanuel.boss@maine.edu)

2169-9275/13/10.1002/jgrc.20109

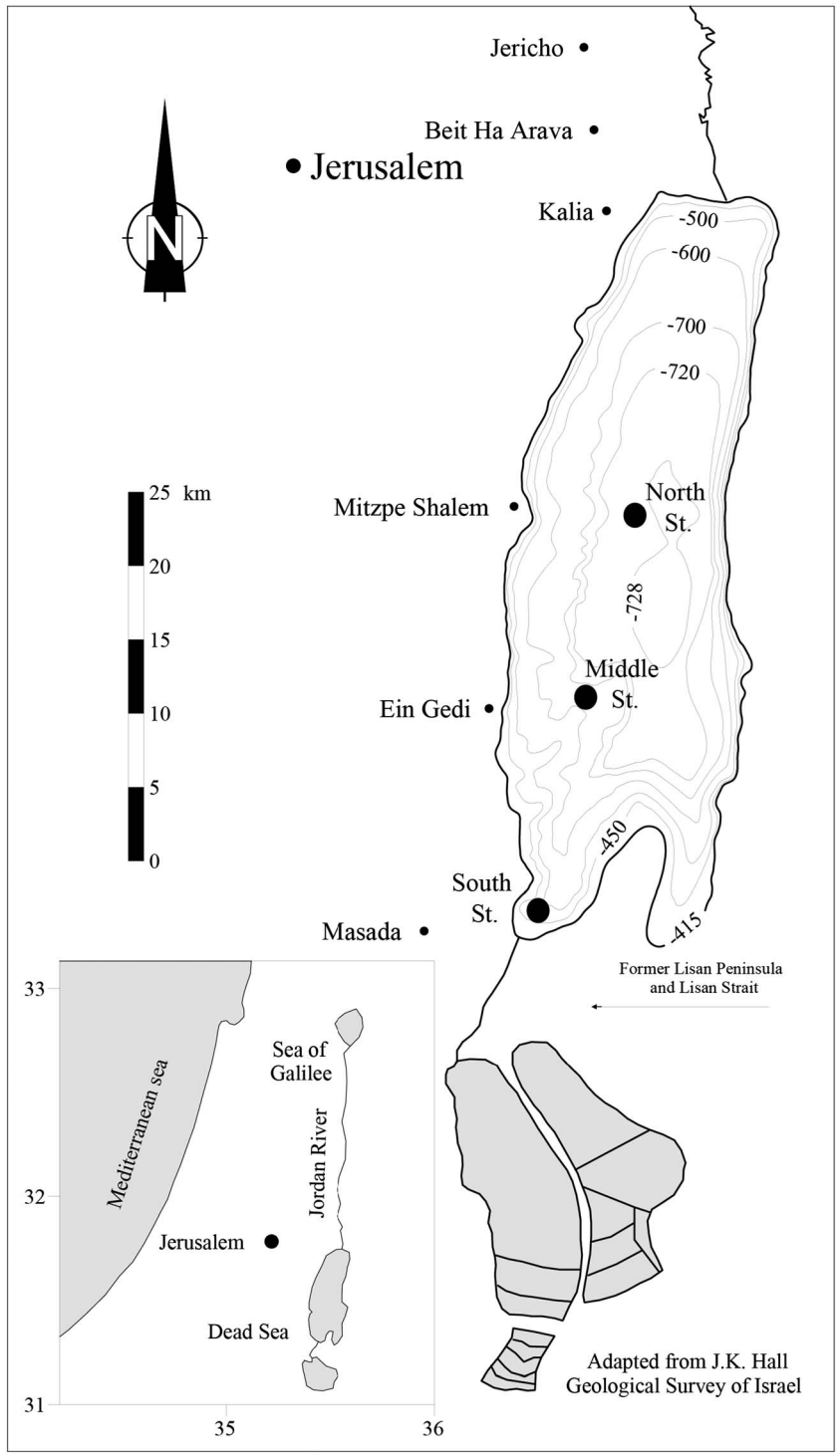

Figure 1. Location of the Dead Sea and the three stations sampled (black dots). This figure is a slightly modified figure of Gertman and Hecht (*J. Mar. Sys., 35*, The Dead Sea hydrography from 1992 to 2000, p. 170, 2002), with permission from Elsevier. Depths are given relative to mean sea level.

the laboratory measurements, we were able to process the field data and obtain, for the first time, a comprehensive distribution of the lake optical properties.

2. Methods

[5] The lake was sampled from the R/V *Sivan* using a battery-powered self logging profiling package. All measurements were carried out during the day within 4 h of local noon.

2.1. Profiling Package

[6] An inherent optical properties package containing a WETLabs ac-9 (412, 440, 488, 510, 532, 555, 650, 676, 715 nm), a WETLabs Eco-VSF (440 nm), a SeaBird CTD (SBE-19Plus), a pump, and a WETLabs DH4 data logger was profiled in the Dead Sea at three different locations (Figure 1). The conductivity sensor of the conductivity-temperature-depth (CTD) did not provide usable data due

to it being out of range, and hence we do not present estimates of salinity. The southern station was shallow (~30 m) and near the southern end of the lake overlooking the pipeline connecting the lake with the evaporation ponds of Dead Sea Works at the southern basin of the lake. The two other stations (middle and northern) were deep (>250 m depth). The package was profiled with and without a 0.2 μm filter (Gelman SuporCap) so that the properties of particulate and dissolved materials could be separated. In addition, by taking the difference between the two measurements, we obtained particulate properties that are calibration independent [*Boss et al*., 2007; *Slade et al*., 2010] (see below). This procedure assumes that colored dissolved organic matter (CDOM) distribution is not changing between consecutive profiles. This assumption is likely robust in an environment such as the Dead Sea, away from sources of CDOM variability such as rivers inlets (sinks of CDOM, such as photooxidation, operate on time scales of weeks). Indeed, our results (see below) show that CDOM is horizontally homogenous in the lake, to within the uncertainties of our measurements.

[7] The package was turned on and lowered to about 10 m for 5 min to warm-up the instruments, debubble, and acclimate to the local conditions. It was then brought back to the surface and profiled using a winch at a rate of nearly 0.5 m s^{-1}.

[8] At the middle station a LISST-100 (Type B) was also deployed. The LISST had an uncalibrated pressure sensor that was used to determine the depth of the measurements (vicariously calibrated using the fact that the first measurements were within 1 m below the surface while deepest measurements were at 200 m). The LISST was parked at fixed depths for approximately 1 min so that O(100) measurements could be averaged, decreasing the uncertainty in the mean particulate size spectra. The depth interval was 3 m from surface to 30 m and a 10 m interval below. LISST measurements can suffer from contamination by ambient light at shallow depths (most affected are the outer rings, likely affecting inversion for the concentration of small particles [*Andrews et al*., 2011]). Given the levels of illumination and attenuation in the Dead Sea (800 W m^{-2}, 0.1 m^{-1}, respectively, for April [*Oren and Shilo*, 1982; *Kudish et al*., 2005] see section 3.3 below), and *Andrews et al*. [2011] assertion that the effect is only observed for PAR > 30 W m^{-2}, upper layer ($z < 32$ m) size data regarding small particles could be overestimated.

[9] Comparisons between different stations and between multiple profiles within a station provide us a measure of the uncertainties in the measurements (due, for example, to instrumental drift or processing procedure).

2.2. Data Processing

[10] The data from the various sensors were merged in time into a single file using the timestamp provided to each data point by the data logger. Prior to merging, a three-point median filter was applied to remove spikes from the ac-9 data. CTD pressure was tared and offset to be colocated with the position where water was pumped into the ac-9 and where the backscattering measurements were carried out (0.9 m from the top of the cage). Pressure (P) was converted to depth assuming a constant density for the Dead Sea, $\rho = 1240$ kg m^{-3}, and using the hydrostatic approximation, $z = P/(\rho \cdot 9.81\ \mathrm{ms}^{-2}) = P[\mathrm{db}]/1.216$. The associated uncertainty in depth is less than 5% (based on density stratification in the Dead Sea [e.g., *Gertman and Hecht*, 2002]).

[11] Data from the downward profile were median-binned into 1 m intervals and calibration offsets were applied based on the median of six absorption and nine attenuation calibrations performed within 2 days of the measurements. Up-cast data was discarded, due to interaction with the wake of the package prior to measurement. Uncertainty in the calibrations values, estimated from their standard deviation ranged spectrally from 0.01 to 0.02 m^{-1} for absorption and from 0.02 to 0.03 m^{-1} for attenuation with largest uncertainties in blue wavelengths. Given the larger uncertainties in the calibration coefficients for the attenuation measurements, CDOM was inferred using the absorption measurements (attenuation measurements were consistently about 0.02 m^{-1} lower than those of absorption).

2.2.1. Particulate Absorption and Attenuation Coefficients (ac-9)

[12] Particulate absorption and attenuation were calculated from the difference between 1 m binned total and dissolved measurements conducted in two consecutive profiles, resulting in properties that are calibration, temperature, and salinity independent [*Boss et al*., 2007].

[13] The resultant absorption spectrum was featureless but needed to be corrected for scattering. Given that the absorption spectra were expected to be dominated by nonalgal particles (NAP), whose spectra are nearly decreasing exponentials [e.g., *Babin et al*., 2003], we did not want to assume a lack of absorption at 715 nm, the longest wavelength available with the ac-9 [e.g., *Zaneveld et al*., 1994]. We used the proportional method of *Zaneveld et al*. [1994] (removing a constant proportion of scattering from absorption), but rather than assume the magnitude of scattering contribution, we find its contribution (denoted by ε below) by performing the following fit to the measured absorption spectra $a_{p,measured}(\lambda)$ using an implicit model and the fact that the scattering coefficient is the difference between measured attenuation ($c_{p,measured}(\lambda)$) and corrected absorption ($a_{p,corrected}(\lambda)$)

$$a_{p,corrected}(\lambda) = a_{p,measured}(\lambda) - \varepsilon\left(c_{p,measured}(\lambda) - a_{p,corrected}(\lambda)\right) \quad (1)$$

[14] In this model, we initially assume that the estimated corrected absorption ($\widetilde{a}_{p,corrected}(\lambda)$) is approximated by a decreasing exponential (of unknown slope), $\widetilde{a}_{p,corrected}(\lambda) = \hat{a}_p(440)e^{-s_d(\lambda-440)}$, which after an algebraic manipulation yields

$$\hat{a}_p(440)e^{-s_d(\lambda-440)}(1-\varepsilon) + \varepsilon c_{p,measured}(\lambda) = a_{p,measured}(\lambda). \quad (2)$$

[15] This is a system of nine equations (one per wavelength) with three constant unknowns ($\hat{a}_p(440)$ [m^{-1}], s_d [nm^{-1}], ε).

We solve this system via a nonlinear least-squares minimization using measurements at only the seven shortest wavelengths of the ac-9 (to avoid potential errors associated with differences at any given depth between temperature and salinity in filtered and unfiltered profiles). The solution is the best fit in a least-squares sense (this is an over-constrained problem). Once we have the three constants we compute the corrected absorption from

$$a_{p,corrected}(\lambda) = a_{p,measured}(\lambda) - \varepsilon\left(c_{p,measured}(\lambda) - a_{p,corrected}(\lambda)\right)$$
$$\rightarrow a_{p,corrected}(\lambda) = \frac{a_{p,measured}(\lambda) - \varepsilon c_{p,measured}(\lambda)}{1-\varepsilon}. \quad (3)$$

[16] We found that $\varepsilon \in [0.16,0.23]$, consistent with previous estimates [e.g., *Zaneveld et al.*, 1994]. Note that this procedure is designed to correct the absorption signal for contamination by scattering (by solving for ε). It *does not* force the signal to be a decreasing exponential (which, however, we do find to fit well the data, see Results and Discussion).

2.2.2. Dissolved Absorption Coefficients (ac-9)

[17] Dissolved properties were computed from measurements with 0.2 μm filters positioned at the intakes of the ac-9. However, given the higher confidence in the a-side calibrations, we used only the 0.2 μm measurements through the a-side of the ac-9 ($a_{0.2\ \mu m,measured}(\lambda)$) to estimate CDOM. We corrected for transmission effects at the windows (see (A1) in appendix A for computation of $T_{\mathrm{SW\text{-}G}}(\lambda)$, $T_{\mathrm{DIW\text{-}G}}(\lambda)$, which denote the transmission between salt-water and glass or deionized water and glass, respectively) and scattering by salts as follows:

$$a_{CDOM}(\lambda) = a_{0.2\,\mu m,measured}(\lambda) - 0.166 b_{salts}(\lambda) - \frac{0.2}{0.25\,m} log\left(\frac{T_{SW\text{-}G}(\lambda)}{T_{DIW\text{-}G}(\lambda)}\right), \quad (4)$$

where scattering by salts (b_{salts} (λ)) was computed from *Zhang and Hu* [2009], assuming $S = 270\ \mathrm{g\ kg^{-1}}$ (see below, section 3.4), ambient temperature, and with 0.166 accounting for the portion of scattering collected by the ac-9's a-side detector [*Sullivan et al.*, 2006]. Values at 650, 676, and 715 were replaced by fitting $a_{CDOM}(\lambda)$ at shorter wavelength using an exponential fit (from which the spectral slope of CDOM, s_g, was computed), and extrapolating to the longer wavelengths. This avoids the problems associated with temperature and salinity effects on water absorption at those wavelengths (see below).

2.2.3. Particulate Backscattering Coefficient (Eco-VSF)

[18] We computed the backscattering coefficient at 440 nm using the Eco-VSF following the protocol as in *Boss et al.* [2004], using *Zhang and Hu* [2009] to compute the backscattering by dissolved salts assuming $S = 270\ \mathrm{g\ kg^{-1}}$ (see below), integrating over the three angular measurements. *Boss et al.* [2004] proposed that the uncertainty is on the order of 10% based on closure between different instruments measuring backscattering in different ways at a coastal area. Effects of dissolved salt on the angle of scattering (through refraction of the light beams at the instrument-water interface) are likely to add some additional small uncertainties to this value.

2.2.4. Particulate Size Distribution and Beam Attenuation at 670 nm (LISST)

[19] We added $0.06\ \mathrm{m^{-1}}$ to the attenuation measured by the LISST to account for transmission offset and salt scattering based on the offset we observed in the lab with Dead Sea waters (based on lab measurements with a sample from Dead Sea water and consistent with theory, e.g., Appendix A, to within the uncertainty of the measurement). We used both spherical [*Agrawal and Pottsmith*, 2000] and nonspherical [*Agrawal et al.*, 2008] inversions to obtain particulate size distribution (PSD) from the near-forward scattering measurements of the LISST.

[20] To assess how the LISST inversion may be affected by the high index of refraction of the water, we mixed precision-size beads in both DIW and 0.2 μm filtered Dead Sea water and compared the size distributions obtained (beads varying from 2 to 90 μm). The two size distributions agreed well differing at most by one size bin in the assignment of the peak size (not shown).

3. Results and Discussion

[21] The Dead Sea exhibited a 1.5°C strong thermocline separating the upper layer from the isothermal layer below (Figures 2–4, upper-left panels). Having no salinity measurements, we do not know the density distribution. Based on bi-monthly measurements conducted in previous years [*Gertman and Hecht*, 2002], temperature and density stratification have a similar pattern. Optical properties are nearly constant below 30 m while varying continuously in the upper layer, suggesting variance in optical properties is driven by near-surface processes (Aeolian input, rain and rivers input). The relatively weak stratification in all properties suggests that the lake has gone through winter overturning earlier that winter.

3.1. Particulate Properties

[22] Particulate absorption resembled that of NAP having little in way of spectral features and decreasing exponentially from blue to red (Figures 2–4), thereby confirming our assumption in the model used to estimate the proportion of scattering in the measured absorption (equation (2)). Spectral slopes of particulate absorption were found to be $s_d \sim 0.009$–$0.015\ \mathrm{nm^{-1}}$ consistent with oceanic NAP, increasing toward the surface. These results lack the typical chlorophyll *a* absorption peak at 676 nm and shoulder near 488 nm found in the surface of ocean and lakes, suggesting the lack of photosynthetic organisms in the water column when we sampled. Particulate beam attenuation is featureless as well, being well fitted by a power-law function.

[23] Particulate attenuation and absorption were significantly higher at the shallow southern station than at the two other stations. They are also higher in the surface layer compared to at depth with a sharp narrow peak value at the thermocline (~20 m). Values of the spectral slope of particulate attenuation (γ, the exponent of the power-law fit) varied from 0.15 (±0.1) at depth to 0.65 (±0.1) near the surface, consistent with smaller average particle size near the surface than at depth. The particulate backscattering ratio varied between 0.011–0.016 (±0.001) and decreased with depth suggestive of less refractive particles with depth, though the magnitude of difference could be explained from the change in mean particle size [*Twardowski et al.*, 2001, Figures 1a and 9]. Halite crystals have an index of refraction relative to salt water with $270\ \mathrm{g\ kg^{-1}}$ (see below, computed based on *Quan and Fry* [1995]) of about 1.11 similar to that of desert dust, a likely source of particles to the Dead Sea [*Wagner et al.*, 2012]. It is therefore unlikely that the particulate backscattering ratio will reflect changes in particulate composition.

[24] The beam attenuation of the LISST, deployed only at the middle station, had a similar trend with depth as that of the ac-9 (Figure 5). It is, however, significantly higher (by nearly a factor of 3), which is consistent with its acceptance angle being much smaller [*Boss et al.*, 2009], and of magnitude previously observed [*Neukermans et al.*, 2012]. The explanation for this discrepancy is the presence of a significant population of large particles (>30 μm), which do not affect the ac-9 attenuation measurements as much as the LISST [*Boss et al.*, 2009]. Indeed, the LISST-based PSDs (Figure 5) show the presence of a population of large particles at all depths. The relative contribution of this population is increasing with depth. The increase of size with depth is also

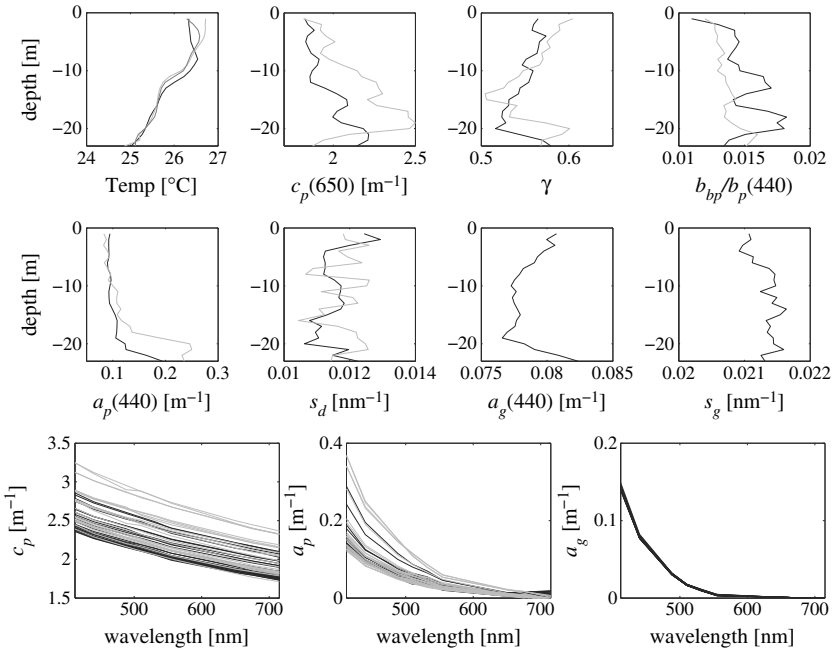

Figure 2. Temperature and inherent optical properties of particles and dissolved materials at the southern station, near the outlet of the evaporation ponds. From left to right and top to bottom the properties displayed are: temperature, beam-attenuation at 650 nm, spectral-slope of beam attenuation, particulate backscattering ratio, particulate absorption at 440 nm, spectral slope of particulate absorption, dissolved absorption at 440 nm, spectral slope of dissolved absorption, particulate beam attenuation spectra, particulate absorption spectra and dissolved absorption spectra. We have two estimates of particulate properties (grey and black lines) based on the difference between two casts performed within 12 min of each other where total measurements were taken, and one cast performed in between them, where the dissolved properties were measured.

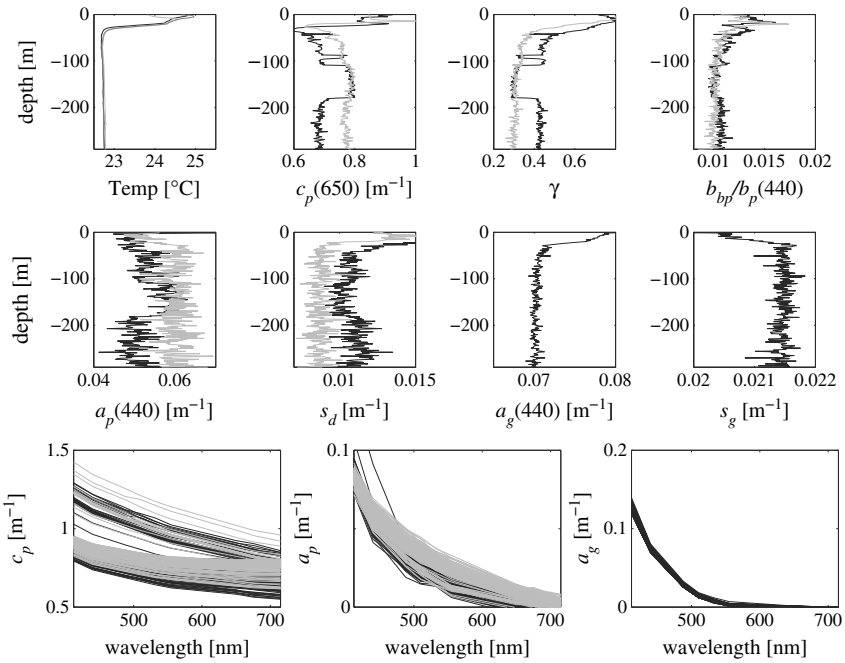

Figure 3. Same properties as in Figure 2 but for the northern station. We have two estimates of particulate properties based on the difference between two casts performed within 45 min of each other where total measurements were taken, and one cast performed in between them, where the dissolved properties were measured. Note that while both profiles reveal a similar range of properties, both exhibit significantly different distributions of beam attenuation. Large discontinuities in the black profile are inconsistent with other properties and suggest an artifact of sampling.

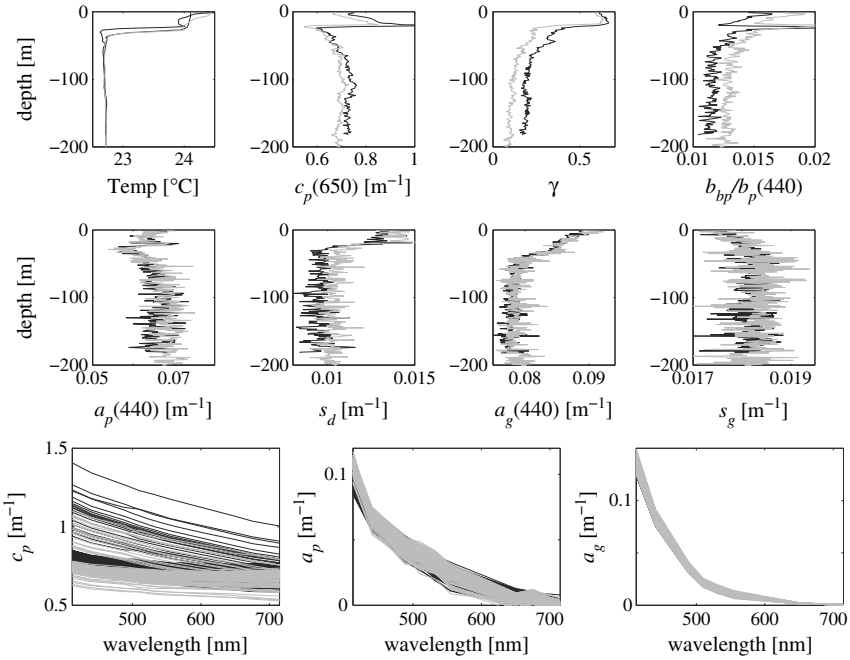

Figure 4. Same properties as in Figure 2 but for the middle station. We have two estimates of particulate properties based on the difference between two casts performed within 3 h of each other where total measurements were taken, and two casts performed in-between them, where the dissolved properties were measured. Differences between values here and in Figure 3 provide an estimate of uncertainty, as we do not expect large gradients in optical properties at depth.

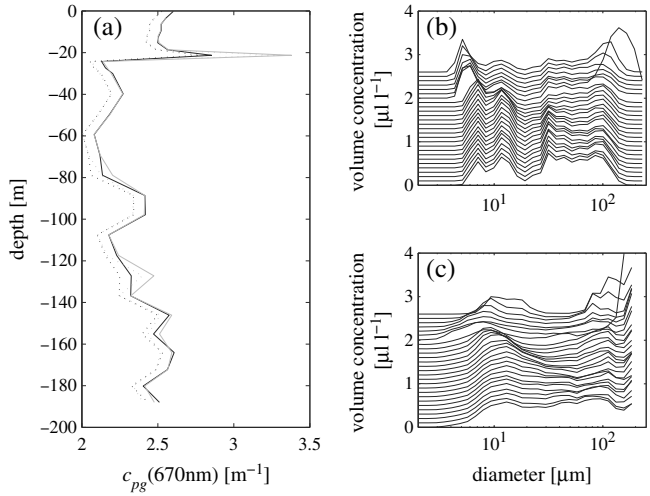

Figure 5. LISST Beam attenuation at 670 nm (left panel). Solid lines denote average while dashed line denotes medians processed with a pre- (black line) and post (grey) calibration. Volume concentration as inverted from LISST measurements (right panels), using the standard (spherical) inversion (top) and nonspherical inversion (bottom). The curves represent particle volume distribution from different depths with top being near surface and bottom ~190 m depth. Each curve is offset by 0.1 µl l^{-1} from the next, and was taken at an interval of approximately 3 m in the top 30 m and 10 m below. Note that PSDs above 32 m could have suffered from contamination with ambient light [*Andrews et al.*, 2011]. The outlier PSD originates from the thermocline (~20 m) where a strong Schlieren effect may have been present [*Mikkelsen et al.*, 2008].

consistent with the trend observed with the spectral slope of particulate attenuation (γ). The size of particles observed and the increase of size with depth is consistent with previous report of sediments trap deployed in the Dead Sea [*Stiller et al.*, 1997] where, during certain periods, precipitating halite were large in size and dominated the sedimenting particles. Note that LISST PSDs above 32 m could have suffered from contamination with ambient light, which would be most

pronounced in the inversion of small particles [*Andrews et al*., 2011].

[25] Large beam attenuation values at the base of the thermocline could be the result of accumulation of large particles on a density discontinuity. However, the outlier PSD inverted there (Figure 5) suggests that it may have been an artifact due the strong change in water index of refraction, causing the instrument's beam to fluctuate away from the detector as was observed before at large density discontinuities [*Mikkelsen et al*., 2008].

3.2. Dissolved Properties

[26] Dissolved absorption values were very consistent throughout the Dead Sea, having amplitude that varied by less than 20% from surface to 300 m depth, being higher at the surface layer (Figures 2–4). Spectral slope was relatively high ($0.02 \pm 0.002\,\mathrm{nm}^{-1}$), increasing with depth. The lower spectral slope and higher absorption values near the surface were consistent with the surface CDOM having higher molecular weight, more labile compared to material at depth [*Yacobi et al*., 2003].

3.3. Comparison With Historical Data

[27] The only published optical data we are aware of were collected using a PAR radiometer [*Oren and Shilo*, 1982, Figure 4] spanning April to October of 1980 and collected near the middle station. The diffuse attenuation of PAR based on fitting a line to these measurements is $0.1 \pm 0.01\,\mathrm{m}^{-1}$, which is consistent (through a conversion to the diffuse attenuation at 490 nm ($k_d(490)$, see *Morel et al*. [2007]) with the absorption and backscattering measurements we obtained in the current study ($k_d(490) \sim [a(490) + b_b(490)]/0.8 = 0.1 \pm 0.02\,\mathrm{m}^{-1}$, Figures 3 and 4, with 0.8 being an approximation to the averaged cosine of the incident light).

3.4. Laboratory Analysis of Hyper-Spectral Dissolved Spectra

[28] A surface sample from the Dead Sea collected on 5/1/2012 near the southern station (Figure 1) was sent to the University of Maine for analysis (conducted on 5/8/2012). The sample was stored in an opaque plastic container at room temperature. The sample was filtered through a 0.2 µm filter and density was measured to be $1242\,\mathrm{kg\,m}^{-3}$ consistent with previous accounts of Dead Sea density [*Steinhorn*, 1983; *Gertman and Hecht*, 2002].

[29] *Sullivan et al*. [2006] conducted measurement of the effect of a salt (NaCl) on attenuation and absorption of water using a WET Labs ac-S and tabulated their results as function of wavelength. While *Sullivan et al*. [2006] accounted for scattering by dissolved salts, they did not *explicitly* account for changes in transmission at the window/water interface. Because the transmission term (third term in equation (A6)) is highly linear as function of salinity, it should already be well captured in those tables and, using those tables, we do not need to account for it explicitly.

[30] Using *Sullivan et al*. [2006] tables for salinity and temperature specific absorption and attenuation of water ($\psi_{a,S}, \psi_{c,S}, \psi_T$), and *Zhang and Hu* [2009] values for salt scattering ($b_{Salt}(S,\lambda)$), we can write expressions for measured attenuation and absorption of dissolved material by the ac-S as a function of concentration of salts (S, [$\mathrm{g\,kg}^{-1}$]) and taking account of temperature effects (ΔT):

$$\begin{aligned} c_{0.2\mu m}(\lambda) - c_{DIW}(\lambda) &= A(440)e^{-s_g(\lambda-440)} + b_{Salt}(S,\lambda) \\ &\quad + S\psi_{c,s}(\lambda) + \Delta T\psi_T(\lambda) \\ a_{0.2\mu m}(\lambda) - a_{DIW}(\lambda) &= A(440)e^{-s_g(\lambda-440)} + 0.166 b_{Salt}(S,\lambda) \\ &\quad + S\psi_{a,s}(\lambda) + \Delta T\psi_T(\lambda). \end{aligned} \tag{5}$$

[31] The 0.166 term account for the 41.7° forward scattered light that is collected by the absorption-side detector of the ac-S. While temperature has the strongest effect on attenuation and absorption in the near-infrared, salinity effects are large around 620 nm and scattering by dissolved salts is important in the blue [*Sullivan et al*., 2006].

[32] The surface sample from the Dead Sea was filtered through a 0.2 µm filter and gently gravity fed through the ac-S. The distinctive salinity signature was observed in the 620–670 nm spectral range and the strong effect of temperature (Figure 6). We decomposed these spectra using a best-fit optimization of the ac-S dissolved data to the model (equation (5)), assuming constant spectral slope of CDOM ($s_g = 0.02\,\mathrm{nm}^{-1}$), no scattering by salt water and solving for T, S, and $A(440)$. We then computed the scattering by salts from *Zhang and Hu* [2009] for a temperature of 20°C, input it back into (equation (4)) and recomputed T, S, and $A(440)$.

[33] We then used these T and S to compute the dissolved attenuation and absorption (c_g and a_g) from

$$\begin{aligned} c_g(\lambda) &= c_{0.2\mu m}(\lambda) - c_{DIW}(\lambda) - b_{Salt}(S,\lambda) \\ &\quad - S\psi_{c,s}(\lambda) - \Delta T\psi_T(\lambda) \\ a_g(\lambda) &= a_{0.2\mu m}(\lambda) - a_{DIW}(\lambda) - 0.166 b_{Salt}(S,\lambda) \\ &\quad - S\psi_{a,s}(\lambda) + \Delta T\psi_T(\lambda). \end{aligned} \tag{6}$$

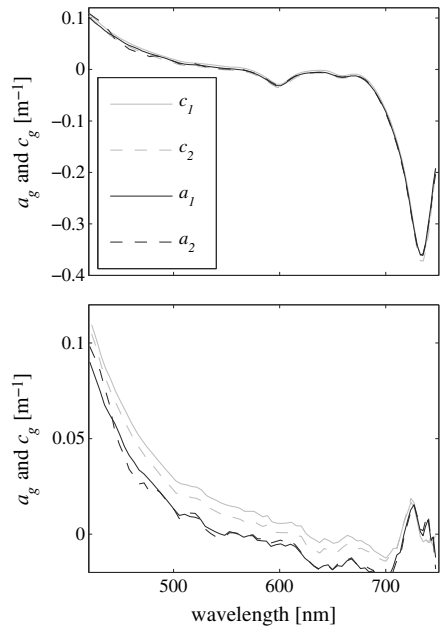

Figure 6. Duplicate measurements of dissolved attenuation and absorption of Dead Sea waters corrected only for DIW offset (top panel) and corrected, additionally, for temperature and salinity effects (bottom panels). Differences between spectra provide a sense of the uncertainty in the correction and in the aggregate uncertainties associated with the salinity and temperature corrections.

[34] We found that it was not necessary to iterate further (difference was smaller than standard deviation between replicate) and that $S = 270 \pm 7\ \mathrm{g\,kg^{-1}}$, and $\Delta T = -27.9 \pm 0.6\,^{\circ}\mathrm{C}$. Varying CDOM slope from 0.015 to $0.02\ \mathrm{nm^{-1}}$ in equation (5) resulted in negligible differences. The CDOM values obtained (c_g and a_g) are similar in magnitude to those we observed in 2004 (compare bottom panels of Figures 6 and 2).

[35] The salinity value obtained ($270\ \mathrm{g\,kg^{-1}}$) was within 2% of the value reported in *Steinhorn* [1983] ($276\ \mathrm{g\,kg^{-1}}$ for density of $1233\ \mathrm{kg\,m^{-3}}$), suggesting that the measurements of dissolved absorption/attenuation and their decomposition (equations (5)–(6)) based on inputs from *Sullivan et al.* [2006] and *Zhang and Hu* [2009], could provide useful salinity information, despite: (1) the fact that *Sullivan et al.* [2006] table is based on a solution of NaCl. (2) The fact the *Sullivan et al.* [2006] study only measured properties up to $100\ \mathrm{g\ kg^{-1}}$ and that *Zhang et al.*'s results were intended to be used below $120\ \mathrm{g\,kg^{-1}}$. The high temperature offset observed ($\sim -28\,^{\circ}\mathrm{C}$) compared to the calibration fluid suggests that the effects of dissolved salts and temperature on water absorption are not independent (see discussion in *Sullivan et al.* [2006]).

3.5. Effects of Dissolved Salts on Inherent Optical Properties and Their Measurements

[36] The specific composition of the dissolved salts makes a difference both for the optical properties of the mixture (e.g., index of refraction and scattering [*Zhang et al.*, 2009]) and for its physical properties (e.g., density [*Anati*, 1999]). Differences between NaCl and Dead Sea brines are on the order of 15% for water-salt mixture density determination [*Zhang et al.*, 2009; *Anati*, 1999]. In addition, scattering by salts is not a linear function of their concentration but rather has a negative second derivative with increasing salt concentration [*Zhang and Hu*, 2009; *Zhang et al.*, 2009]. It was thus somewhat surprising that observation of the effect of salinity on water absorption and attenuation at red wavelength provided an estimate of salinity within a few percent of observed density-salinity relationship for the Dead Sea when salinity was computed using tables based on NaCl.

[37] Assuming a salinity of $270\ \mathrm{g\,kg^{-1}}$ and that *Sullivan et al.* [2006] and *Zhang et al.* [2009] (which uses the index of refraction formulation of *Quan and Fry* [1995]) formulations are applicable for Dead Sea water, the largest bias in attenuation and absorption is negligible below 600 nm, positive O($0.002\ \mathrm{m^{-1}}$) near 610 nm, and negative and O ($0.008\ \mathrm{m^{-1}}$) near 725 nm. Scattering due to salts is O ($0.002\ \mathrm{m^{-1}}$) at 400 nm decreasing as wavelength to the power of –4 to the red. With respect to measurement biases, transmission offsets with a 25 cm transmissometer are on the order of $-0.011\ \mathrm{m^{-1}}$ at all wavelengths while being five times larger for the LISST (see appendix A). Compared to the optical properties of the lake, these values are generally small (<10% at visible wavelengths (<700 nm)).

4. Summary

[38] This paper presents the first observations of inherent optical properties conducted in the Dead Sea. Absorption spectra of dissolved and particulate materials are consistent in their spectral shape with those observed in the oceans and in freshwater lakes, with, however, one major difference: the lack of observable phytoplankton pigment absorption near the surface. Attenuation spectra are also consistent with observations from other aquatic environments, exhibiting power-law like spectra. A large decrease in spectral slope of particulate attenuation is observed with depth with relatively little change in attenuation magnitude. The likely cause is the formation of larger particles with depth (consistent with LISST observations), most likely due to halite precipitation [*Anati*, 1993; *Gavrieli*, 1997; *Stiller et al.*, 1997]. Lab analysis of the hyperspectral absorption and attenuation spectra of dissolved Dead Sea waters using an in situ spectrophotometer (WETLabs ac-S) supports the use of such measurements in the red and infrared part of the spectrum to monitor the salinity of hyper-saline bodies of water in situ, as traditional in situ methods, such as CTD, do not work.

Appendix A: Effect of Dissolved Salts on Spectrophotometric Measurements

[39] Dissolved salts modify the inherent optical properties of the water in which they are dissolved [*Morel*, 1974; *Zhang and Hu*, 2009; *Sullivan et al.*, 2006]. In addition, they modify the transmission properties at interfaces [e.g., *Bohren and Huffman*, 1983]. We use theoretical considerations to evaluate how inherent optical properties of hypersaline water can be retrieved from instrumentation for which DIW was used as a blank.

[40] When light goes through a collimated design beam-transmissometer it interacts with two glass-water boundaries. At these boundaries some of the light is reflected backward. The transmission through this boundary, ($T_{\mathrm{G\text{-}W}} = 1 - R_{\mathrm{G\text{-}W}}$, where $R_{\mathrm{G\text{-}W}}$ is reflection at the glass-water interface), depends on the change in index of refraction between glass and water [e.g., *Bohren and Huffman*, 1983], and is independent of the direction of propagation. For a near-perpendicular beam

$$T_{\mathrm{G\text{-}W}} = \frac{4 n_G n_W}{(n_G + n_W)^2} \tag{A1}$$

where n_G and n_W are the indices of refraction of glass and water. The signal arriving at the detector is given by:

$$I(L) = I(0) T^2{}_{\mathrm{G\text{-}W}} e^{-cL}, \tag{A2}$$

where $I(0)$ is the signal leaving the source, c the attenuation coefficient in the medium and L the path-length in the medium.

[41] When a calibration fluid is inserted in the transmissometer (e.g., cleanest deionized water available) the signal at the receiver is

$$I_{DIW}(L) = I(0) T^2{}_{G\text{-}DIW} e^{-c_{\mathrm{DIW}} L} \tag{A3}$$

where $T_{G\text{–}DIW}$ denotes the transmission coefficient between water and glass. When the sample fluid is inserted in the transmissometer (e.g., a sample with material suspended in salt water) the measurement is proportional to:

$$I_{sample}(L) = I(0) T^2{}_{G\text{-}SW} e^{-c_{sample+SW} L} \tag{A4}$$

where $T_{G\text{–}SW}$ denotes the transmission coefficient between salt-water and glass. The ratio of the two measurements (sample and DIW) is used to deduce the attenuation of the sample

$$Tr = \frac{I_{sample}(L)}{I_{DIW}(L)} = \frac{T^2{}_{G\text{-}SW}}{T^2{}_{G\text{-}DIW}} e^{-\left(c_{sample+SW} - c_{DIW}\right) L}. \tag{A5}$$

[42] It follows that the attenuation computed from this transmission is related to the true attenuation of the sample through equation

$$c_{measured} = \frac{log(Tr)}{L} = c_{sample+SW} - c_{DIW} - \frac{2}{L} log\left(\frac{T_{G\text{-}SW}}{T_{G\text{-}DIW}}\right). \quad \text{(A6)}$$

[43] Thus, in order to obtain the sample's attenuation, c_{sample}, we need to correct it for: (1) the attenuation by the salts ($c_{sw} - c_{DIW}$) and (2) transmission changes between calibration waters and sea water (third term on the right hand side of equation (A6)).

[44] During two separate days we performed measurements with Sequoia Scientific's LISST-100X (Type B) of both laboratory DIW and a filtered sample from the Dead Sea. We found that

$$C_{0.2\,\mu m, Dead\ \ Sea} = -0.06 \pm 0.03\, m^{-1}.$$

[45] The large uncertainty is due to the short path-length of the sensor as well as inhomogeneities in the Dead Sea waters, which we have found to spontaneously precipitate visible crystals after filtration over time scales of tens of minutes. The presence of an attenuation offset is due to both scattering by dissolved salts (a positive offset) and transmission effects (negative offset). Absorption due to dissolved material in these waters is negligible at the LISST wavelength (670 nm).

[46] We varied salt concentration, in *Quan and Fry* [1995] and *Zhang and Hu* [2009] formulations of the effect of salt concentration on the index of refraction and scattering (input to equation (A6)), and found the observed LISST offset to be consistent with $S = 200 \pm 100\ \mathrm{g\,kg^{-1}}$. Note that the transmission term dominates (relative to scattering by dissolved salts), contributing more than 97% to the total attenuation at all salinities.

[47] **Acknowledgments**. We thank E. Biton, A. Shepon, T. Berman, and the skipper of the "Sivan" for their help during the cruise. Comments by J. Sullivan, X. Zhang, D. Bowers and an anonymous reviewer have resulted in significant improvements of this paper. Much of the equipment and Boss's work on particulate scattering were funded by the Office of Naval Research. H.G. was supported by The Ministry of Science and Technology.

References

Andrews, S. W., D. M. Nover, K. E. Reardon, J. E. Reuter, and S. G. Schladow (2011), The influence of ambient light intensity on in situ laser diffractometers, *Water Resour. Res.*, *47*, W06509, doi:10.1029/2010WR009841.

Agrawal, Y. C., and H. C. Pottsmith (2000), Instruments for particle size and settling velocity observations in sediment transport, *Mar. Geol.*, *168*, 89–114.

Agrawal, Y. C., A. Whitmire, O. A. Mikkelsen, and H. C. Pottsmith (2008), Light scattering by random shaped particles and consequences on measuring suspended sediments by laser diffraction, *J. Geophys. Res.*, *113*, C04023, doi:10.1029/2007JC004403.

Anati, D. A. (1993), How much salt precipitates from the brines of a hypersaline lake? The Dead Sea as a case study, *Geochim. Cosmochim. Acta*, *57*, 2191–2196.

Anati, D. A. (1999), The salinity of hypersaline brines: Concepts and misconceptions, *Int. J. Salt Lake. Res.*, *8*, 55–70.

Babin, M., D. Stramski, G. M. Ferrari, H. Claustre, A. Bricaud, G. Obolensky, and N. Hoepffner (2003), Variations in the light absorption coefficients of phytoplankton, nonalgal particles, and dissolved organic matter in coastal waters around Europe, *J. Geophys. Res.*, *108*, 3211, doi:10.1029/2001JC000882.

Bohren, C. F., and D. Huffman (1983), Absorption and Scattering of Light by Small Particles, John Wiley, New York.

Boss, E., W. S. Pegau, M. Lee, M. Twardowski, E. Shybanov, G. Korotaev, and F. Baratange (2004), Particulate backscattering ratio at LEO 15 and its use to study particle composition and distribution, *J. Geophys. Res.*, *109*, C01014, doi:10.1029/2002JC001514.

Boss, E., R. Collier, G. Larson, K. Fennel, and W. S. Pegau (2007), Measurements of spectral optical properties and their relation to biogeochemical variables and processes in Crater Lake National Park, OR, *Hydrobiologia*, *574*, 149–159.

Boss, E., W. H. Slade, M. Behrenfeld, and G. Dall'Olmo (2009), Acceptance angle effects on the beam attenuation in the ocean, *Opt. Express*, *17*, 1535–1550.

Boss, E., W.S. Pegau, W.D. Gardner, J.R.V. Zaneveld, A.H. Barnard, M.S. Twardowski, G.C. Chang, and T.D. Dickey (2001), Spectral particulate attenuation and particle size distribution in the bottom boundary layer of a continental shelf, *J. Geophys. Res.*, *106*, 9509–9516, doi:10.1029/2002JC001514.

Gavrieli, I. (1997), Halite deposition in the Dead Sea: 1960-1993, in The Dead Sea - The Lake and its Setting, edited by T. Niemi, Z. Ben-Avraham, and J. R. Gat, pp. 161–170, Oxford University Press, Oxford, U.K.

Gavrieli, I., A. Starinsky, and A. Bein (1989), The solubility of halite as a function of temperature in the highly saline Dead Sea brine system, *Limnol. Oceanogr.*, *34*, 1224–1234.

Gavrieli, I., N. G. Lensky, Y. Dvorkin, I. Gertman, and V. Lyakovsky (2006), The Dead Sea: a highly disturbed water balance, outcomes and possible solutions, *Geophys. Res. Abstr.*, *8*, 02669.

Gertman, I., and A. Hecht (2002), The Dead Sea hydrography from 1992 to 2000, *J. Mar. Sys.*, *35*, 169–181.

Kudish, A. I., V. Lyubansky, E. G. Evseev, and A. Ianetz (2005), Statistical analysis and inter-comparison of the solar UVB, UVA and global radiation for Beer Sheva and Neve Zohar (Dead Sea), Israel, *Theo. Appl. Clim.*, *80*, 1–15.

Mikkelsen, O. A., T. G. Milligan, P. S. Hill, R. J. Chant, C. F. Jago, S. E. Jones, V. Krivtsov, and G. Mitchelson-Jacob (2008), The influence of schlieren on in situ optical measurements used for particle characterization, *Limnol. Oceanogr. Methods*, *6*, 133–143.

Morel, A. (1974), Optical properties of pure water and pure seawater, in Optical Aspects of Oceanography, edited by N. G. Jerlov, and E. Steeman Nielsen, pp. 1–24, Academic Press, London.

Morel, A., Y. Huot, B. Gentili, P. J. Werdell, S. B. Hooker, and B. A. Franz (2007), Examining the consistency of products derived from various ocean color sensors in open ocean (Case 1) waters in the perspective of a multi-sensor approach, *Remote Sens. Envir.*, *111*, 69–88.

Neukermans, G., H. Loisel, X. Mériaux, R. Astoreca, and D. McKee (2012), In situ variability of mass-specific beam attenuation and backscattering of marine particles with respect to particle size, density, and composition, *Limnol. Oceanogr*, *57*, 124–144.

Oren, A. (1999), Microbiological studies in the Dead Sea: future challenges towards the understanding of life at the limit of salt concentrations, *Hydrobiologia*, *405*, 1–9.

Oren, A., and M. Shilo (1982), Population dynamics of *Dunaliella parva* in the Dead Sea, *Limnol. Oceanogr.*, *27*, 201–211.

Quan X., and E. S. Fry (1995), Empirical equation for the index of refraction of seawater, *Appl. Optics*, *34*, 3477–3480.

Slade, W. H., E. Boss, G. Dall'Olmo, M. R. Langner, J. Loftin, M. J. Behrenfeld, C. Roesler, and T. K. Westberry (2010), Underway and moored methods for improving accuray in measurement of spectral particulate absorption and attenuation, *J. Atmos. Ocean. Tech*, *27*, 1733–1746.

Steinhorn, I. (1983), In situ salt precipitation at the Dead Sea, *Limnol. Oceanogr.*, *28*, 580–583.

Stiller, M., J. R. Gat, and P. Kaushansky (1997), Halite precipitation and sediment deposition as measured in sediment traps deployed in the Dead Sea: 1981-1983, in The Dead Sea - The Lake and its Setting, edited by T. Niemi, Z. Ben-Avraham, and J. R. Gat, pp. 171–183, Oxford University Press, Oxford, U.K.

Sullivan, J. M., M. S. Twardowski, J. R. Zaneveld, C. Moore, A. Barnard, P. L. Donaghay, and B. Rhoades (2006), The hyper-spectral temperature and salinity dependent absorption of pure water, salt water and heavy salt water in the visible and near-IR wavelengths (400-750 nm), *Appl. Optics*, *45*, 5294–5309.

Twardowski, M. S., E. Boss, J. B. Macdonald, W. S. Pegau, A. H. Barnard, and J. R. V. Zaneveld (2001), A model for estimating bulk refractive index from the optical backscattering ratio and the implications for understanding particle composition in case I and case II waters, *J. Geophys. Res.*, *106*, 14,129–14,142, doi:10.1029/2000JC000404.

Wagner R., T. Ajtai, K. Kandler, K. Lieke, C. Linke, T. Muller, M. Schnaiter, and Vragel M. (2012), Complex refractive indices of Saharan dust samples at visible and near UV wavelengths: a laboratory study, *Atmos. Chem. Phys.*, *12*, 2491–2512, doi:10.5194/acp-12-2491-2012.

Yacobi, Y. Z., J. J. Alberts, M. Takacs, and M. McElvaine (2003), Absorption spectroscopy of colored dissolved organic carbon in Georgia (USA) rivers: The impact of molecular size distribution, *J. Limnol.*, *62*, 41–46.

Zaneveld, J. R. V., J. C. Kitchen, and C. M. Moore (1994), The scattering error correction of reflecting-tube absorption meters, Proc. Ocean Optics XII, Monte Carlo, Monaco.

Zhang X., and L. Hu (2009), Scattering by pure seawater at high salinity, *Opt. Express*, *17*, 12685–12691.

Zhang, X., L. Hu, M. S. Twardowski, and J. M. Sullivan (2009), Scattering by solutions of major sea salts, *Opt. Express*, *17*, 19580–19585.